J Mater Sci (2008) 43:3279–3288
DOI 10.1007/s10853-008-2524-2

An in situ approach to synthesize pure phase FAU-type zeolite membranes: effect of aging and formation mechanism

Guangqi Zhu · Yanshuo Li · Hongliang Chen · Jie Liu · Weishen Yang

Received: 13 November 2007 / Accepted: 24 January 2008 / Published online: 11 March 2008

Abstract FAU-type zeolite membranes were prepared on porous α-Al_2O_3 tubes by a two-stage in situ synthesis method. The synthesis was carried out in clear solutions without the aid of seeds or organic templates. The first stage synthesis was devoted to the in situ nucleation of FAU-type zeolite, aiming to induce an evenly covered zeolite layer on the support. In situ aging played an important role at this stage as it suppressed LTA phase and promoted the formation of a continuous zeolite layer. The second stage synthesis was performed in a dilute solution, where the pre-formed zeolite layer went on to grow and became compact. Scanning electron microscopy (SEM) observations show that the membranes were made up of well-shaped intergrown crystals, with the thickness around 7 μm. Pervaporation (a membrane-based separation process in which the liquid components diffuse through a membrane and are subsequently vaporized due to the low-pressure exerted on the permeate side of the membrane) measurements were carried out in a water/ethanol (10/90, w/w) mixture to evaluate the membrane performance. The structural and morphological evolutions of FAU-type zeolite membranes during synthesis were tracked down by X-ray diffraction and SEM. The formation mechanism was illuminated based on the experimental results.

G. Zhu · Y. Li · H. Chen · J. Liu · W. Yang (✉)
State Key Laboratory of Catalysis, Dalian Institute of Chemical Physics, Chinese Academy of Sciences, 457 Zhongshan Road, Dalian 116023, China
e-mail: yangws@dicp.ac.cn
URL: http://yanggroup.dicp.ac.cn/

G. Zhu
Graduate School of Chinese Academy of Sciences, Beijing 100049, China

Introduction

Zeolites are a family of crystalline aluminosilicate materials with well-defined subnanometer pores and play an important role in the chemical industry. The unique properties such as high thermal stability, chemical resistance, adsorption ability, and uniform pore structure, etc., make them ideal candidates for membrane materials. In the past two decades, extensive work has been carried out on the preparation and characterization of various types of zeolite films and membranes [1–3]. Over 14 zeolite structures have been successfully synthesized as zeolite membranes so far [4].

FAU-type zeolite, including NaX (with Si/Al ratio of 1–1.5) and NaY (with Si/Al ratio over 1.5) types, bears a three-dimensional pore structure and 12-member rings with a pore diameter of 0.74 nm. The large pore size and preferential adsorption make FAU-type zeolite membranes capable in the separation of organic mixtures. Many efforts have been made on developing an efficient and reproducible method to prepare high-quality FAU-type zeolite membranes. However, the synthesis encounters the problem that impurity phases, usually P-type zeolite, formed in the zeolite layer and reduced the membrane performance due to its smaller pore size and cubic-to-tetragonal structure transformation under a dry atmosphere or an elevated temperature [5]. In order to prevent the formation of impurity phases, most synthesis methods involve a seeding process to induce the formation of FAU-type zeolite in the subsequent hydrothermal treatment [6–20].

Kusakabe and co-workers [6–10] employed a rub-coating technique to seed NaX or NaY zeolite crystals on α-Al_2O_3 tubes. After hydrothermal treatment, NaY zeolite membranes were obtained which were CO_2-selective. Kita et al. [11, 12] chose dip coating as the seeding technique, and they found that P-type zeolite formed in the zeolite

layer when NaX zeolite crystals were seeded, while pure FAU-type zeolite membranes were obtained when NaY zeolite crystals were seeded. Li et al. [13] used dip coating as well to prepare X-type zeolite membranes that were applied to the separation of 1,3-propanediol from glycerol in aqueous mixtures. Other seeding techniques such as electrophoretic deposition [14] and pulsed-laser deposition [15] have also been reported. In order to avoid the ex situ pretreatment of the support, Clet et al. [16] prepared NaY zeolite membranes on porous stainless steel discs in two steps using seeded and unseeded gel solutions. Besides gel solutions, Kumakiri et al. [17] proposed a clear solution for the secondary growth of the seeded NaY zeolite layer on porous α-Al_2O_3 discs. In their opinion, gel solutions with a large amount of reagents preferred the formation of nuclei in the bulk phase to the growth of seed crystals; on the contrary, dilute clear solutions promoted the growth of seed crystals and made zeolite layers compact. Using the secondary growth strategy, FAU-type zeolite membranes were also synthesized by means of microwave heating [18] and vapor phase transport [19], and good separation results of CO_2/N_2 mixtures were obtained by the latter method.

For all the methods described above, the synthesis suffers from the complexity that usually a high coverage of the support with zeolite crystal seeds has to be achieved; otherwise dome-like defects will arise in the zeolite layers. It would be convenient to use the in situ strategy; in respect of FAU-type, however, the synthesis conditions are stringent so as to avoid the formation of impurity phases. Nikolakis et al. [20] achieved the in situ synthesis of NaX zeolite membranes with the aid of TEAOH, though a long reaction time of 15 days was needed owing to the low reactivity of gel solution.

Here, we present a modified two-stage in situ method [21] to prepare FAU-type zeolite membranes from clear solutions. Artificial seeding process was replaced by the in situ nucleation of FAU-type zeolite on the support, and then the secondary growth was carried out in a dilute solution. Clear solutions were adopted as they win the advantages of homogeneity and high reactivity over gel solutions. The formation of impurity LTA phase was suppressed through the optimization of in situ aging conditions. The structural and morphological evolutions of FAU-type zeolite membranes during synthesis were tracked down by X-ray diffraction (XRD) and scanning electron microscopy (SEM).

Experimental

Membrane synthesis

Porous α-Al_2O_3 tubes (homemade, 9 mm outside diameter, 7 mm inside diameter, 7.5 cm length, ca. 30% porosity) and discs (homemade, 28 mm in diameter, 1.5 mm in thickness, ca. 30% porosity) were used as supports. The surface of support was polished with 1,000 mesh grit-sand paper and then rinsed and sonicated in deionized water several times to remove the loose particles. Before synthesis, the cleaned support was calcined in air at 500 °C for 4 h to burn off the organics on the surface.

Two types of clear solutions, with the molar compositions of $65Na_2O{:}1Al_2O_3{:}10SiO_2{:}2000H_2O$ (S1) and $80Na_2O{:}1Al_2O_3{:}10SiO_2{:}5000H_2O$ (S2), were used for the first and second stage syntheses, respectively. They were both prepared by dissolving sodium hydroxide (96.0%) in deionized water and then adding aluminum foil (99.99%) into the alkaline solution and silica sol (32%, wt.% of SiO_2) at last. The gel solutions that initially formed transformed into clear solutions after stirring for several hours at room temperature, with the turbidity of 2–5 NTU determined by digital photoelectrical turbidimeter (WGZ-200, Shanke Instrument).

A porous α-Al_2O_3 tube was sealed with two Teflon caps at both ends and placed vertically in an autoclave. For the synthesis of the flat membrane, a Teflon holder was used to fix the porous α-Al_2O_3 disc vertically in the autoclave. About 90 mL synthesis solution was added in the autoclave. The first stage synthesis was performed in S1 at 50 °C for 24 h and subsequently at 90 °C for a period (in situ nucleation); the second stage synthesis was performed in S2 at 80 °C for 5 h (secondary growth). After each synthesis, the composite membrane was taken out, thoroughly washed with deionized water and dried at 60 °C overnight. In order to remove the amorphous materials and expose the true crystalline morphology of zeolite layers, selected samples were treated with 0.3 mol/L sodium hydroxide solution at 60 °C for 1 h as soon as the hydrothermal synthesis finished [22].

Membrane characterization

Flat membranes were used to obtain the XRD patterns (Rigaku D/MAX-2500, Cu-K_α radiation, operating at 40 kV and 200 mA), which were processed with MDI Jade 5. In this study, the integrated areas of the (111) peak of FAU phase ($2\theta = 6.1$, $I_{FAU(111)}$) and (200) peak of LTA phase ($2\theta = 7.2$, $I_{LTA(200)}$) were calculated to evaluate each relative content in the zeolite layers, respectively.

The morphology and thickness of the membranes were determined by SEM (Quanta 200 FEG, FEI Company, operating at 30 kV). The compositional analysis was performed by energy-dispersive X-ray spectrometry (EDAX Inc., operating at 30 kV). In order to avoid the interference from α-Al_2O_3 support, the Si/Na molar ratio was used as a direct indication of the corresponding Si/Al molar ratio of each zeolite membrane [22].

Pervaporation measurements

Pervaporation measurements in a water/ethanol (10/90, w/w) mixture were carried out at 65 °C to evaluate the performances of the as-synthesized zeolite membranes. Membrane tubes were sealed in a stainless-steel module with silicone o-rings. Feed was introduced to the outer side of membrane and the lumen was evacuated through a vacuum pump. The permeated gaseous mixture was collected by a trap in liquid nitrogen, weighed and analyzed by a gas chromatography (HP 5890). The membrane performance was evaluated by the total permeation flux (the weight of the permeate collected in per unit of time and membrane area, kg m^{-2} h^{-1}) and separation factor (α). The separation factor was determined as $\alpha_{water/ethanol} = (P_{water}/P_{ethanol})/(F_{water}/F_{ethanol})$, where F_{water}, $F_{ethanol}$, P_{water}, and $P_{ethanol}$ denote the mass fraction of water and ethanol in the feed and permeate sides, respectively.

Results and discussion

In situ nucleation stage

Direct crystallization at 90 °C

At the first stage synthesis, we observed that the zeolite layer, which formed on the support by 4 h of direct crystallization at 90 °C without aging, was not pure FAU phase, as shown in Fig. 1. The peaks at $2\theta = 7.2$, 10.2, 12.5°, etc., were assigned to LTA phase. After the secondary growth, the separation factor $\alpha_{water/ethanol}$ was 30, which was not improved when prolonging the direct crystallization time.

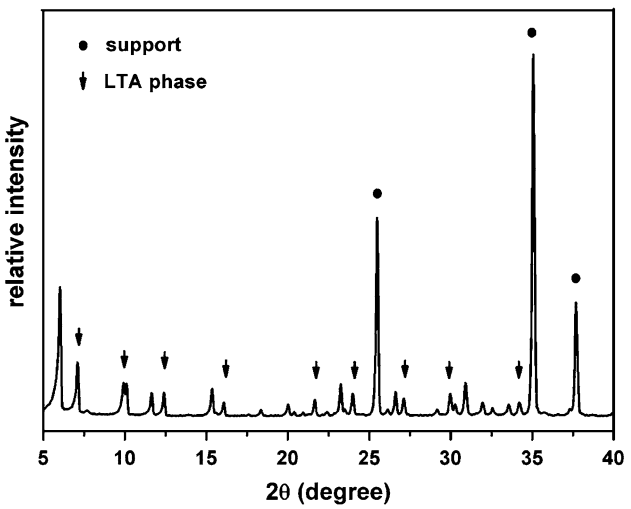

Fig. 1 The XRD pattern of the zeolite layer synthesized at 90 °C for 4 h

Effect of in situ aging temperature and time

Aging is a popular means in the synthesis of zeolite, especially for FAU-type, since it is able to accelerate crystallization, control crystal size, and most of all, suppress impurity phases [23–27]. Recently, aging has been applied to the synthesis of LTA-type and MFI-type zeolite membranes without seeding, which proved to be useful or even necessary as it increased the nucleation density on the support [28–31].

In order to study the effect of aging on the synthesis of FAU-type zeolite membranes, support tubes and solution S1 were co-heated at 30–60 °C for a certain time (in situ aging), followed by crystallization at 90 °C for 4 h. XRD examinations revealed that aging could inhibit the formation of LTA phase, as summarized in Fig. 2. Here, the *y*-axis represents the ratio of $I_{LTA(200)}$ and $I_{FAU(111)}$ ($I_{L/F}$), corresponding to the relative content of LTA phase in the zeolite layers. The $I_{L/F}$ value dropped quickly with the increment of aging time for each aging temperature. The higher applied temperatures, i.e., 50 and 60 °C, were more favorable to reduce the value of $I_{L/F}$. It was noted that a virtually pure phase FAU-type zeolite layer was obtained after aging at 50 °C for 24 h.

The SEM observations proved that a gel layer had deposited onto the support by 8 h of in situ aging at 50 °C (not provided here), with the Si/Na ratio of 0.9. After 24 h, the support was covered by a layer of spherical particles (0.5–1 μm), which turned out to be the aggregates of nano-particles (<30 nm) in the magnified image (Fig. 3a). This layer was incompact and embedded with considerable holes, with the thickness of ca. 4 μm. In the XRD pattern (marked with 0 h in Fig. 4), peaks of FAU phase though low in intensity proved the existence of primary FAU-type zeolite, i.e., the nano-particles aforementioned. Whereas no

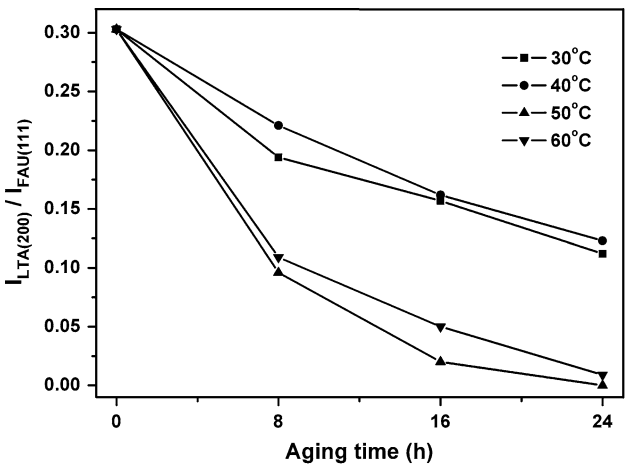

Fig. 2 XRD characteristics of the zeolite layers synthesized with different aging conditions

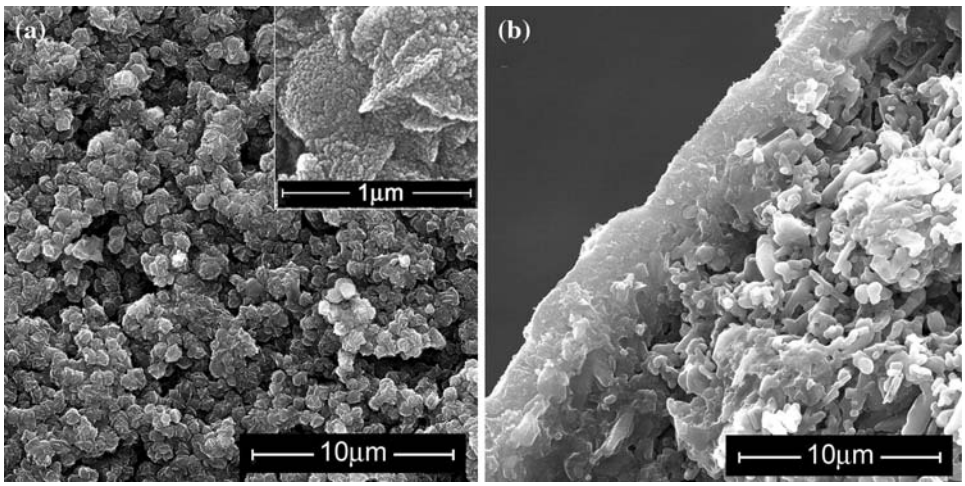

Fig. 3 SEM images of the support after in situ aging at 50 °C for 24 h

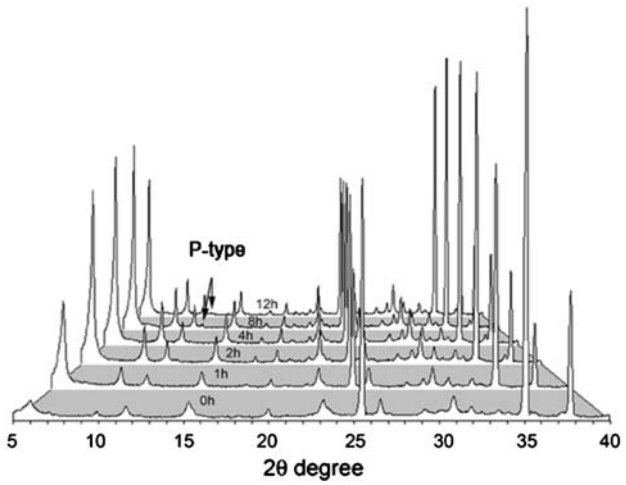

Fig. 4 XRD patterns of the zeolite layers synthesized with different first stage crystallization time

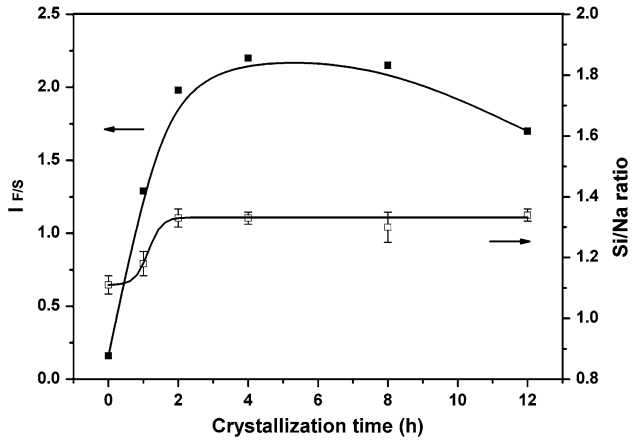

Fig. 5 $I_{F/S}$ and Si/Na ratio as a function of the first stage crystallization time

zeolite phase could be detected even by 20 h, we deduced that the nucleation event took place at the end of aging.

For comparison, "ex situ" aging was also performed to study the necessity of "in situ" aging. Solution S1 was aged solely at 50 °C for 24 h and then the support tube was put in and co-heated at 90 °C for 4 h. XRD examinations (not provided here) show that the powder collected from the synthesis solution was FAU phase, but no zeolite structure could be detected on the support. A similar result was observed during the microwave synthesis of LTA-type zeolite membranes [28].

Effect of the first stage crystallization time

The first stage crystallization was investigated from 0.5 to 12 h. The structural and morphological evolutions of zeolite layers during this process were tracked down by XRD and SEM.

Figure 4 shows the XRD patterns of a series of membranes synthesized with the increasing crystallization time. No impurity phases were detected until 8 h when a low peak at $2\theta = 12.3°$ arose, which was assigned to the (101) peak of P-type zeolite. FAU peaks were greatly enhanced in the first 2 h, and then the change in intensity seemed to be unobvious. The coverage of FAU-type zeolite on the support could be clearly reflected in the intensity ratio of FAU (111) peak and the support peak at $2\theta = 25.5°$ ($I_{F/S}$), as shown in Fig. 5. The $I_{F/S}$ value ascended rapidly at the early stage of crystallization and reached the maximum around 4 h. Further crystallization over 8 h resulted in a decrease in $I_{F/S}$.

Figure 6 shows the SEM images of the zeolite layers synthesized with 1, 2, 4, and 8 h of crystallization, in which b, d, and f were treated with alkali. After 1 h of crystallization, the crystals (0.3–0.5 μm) agglomerated into spherical clusters or large groups, composing a continuous layer with a few voids (Fig. 6a). Some aggregates of nanoparticles similar with the ones formed after in situ aging

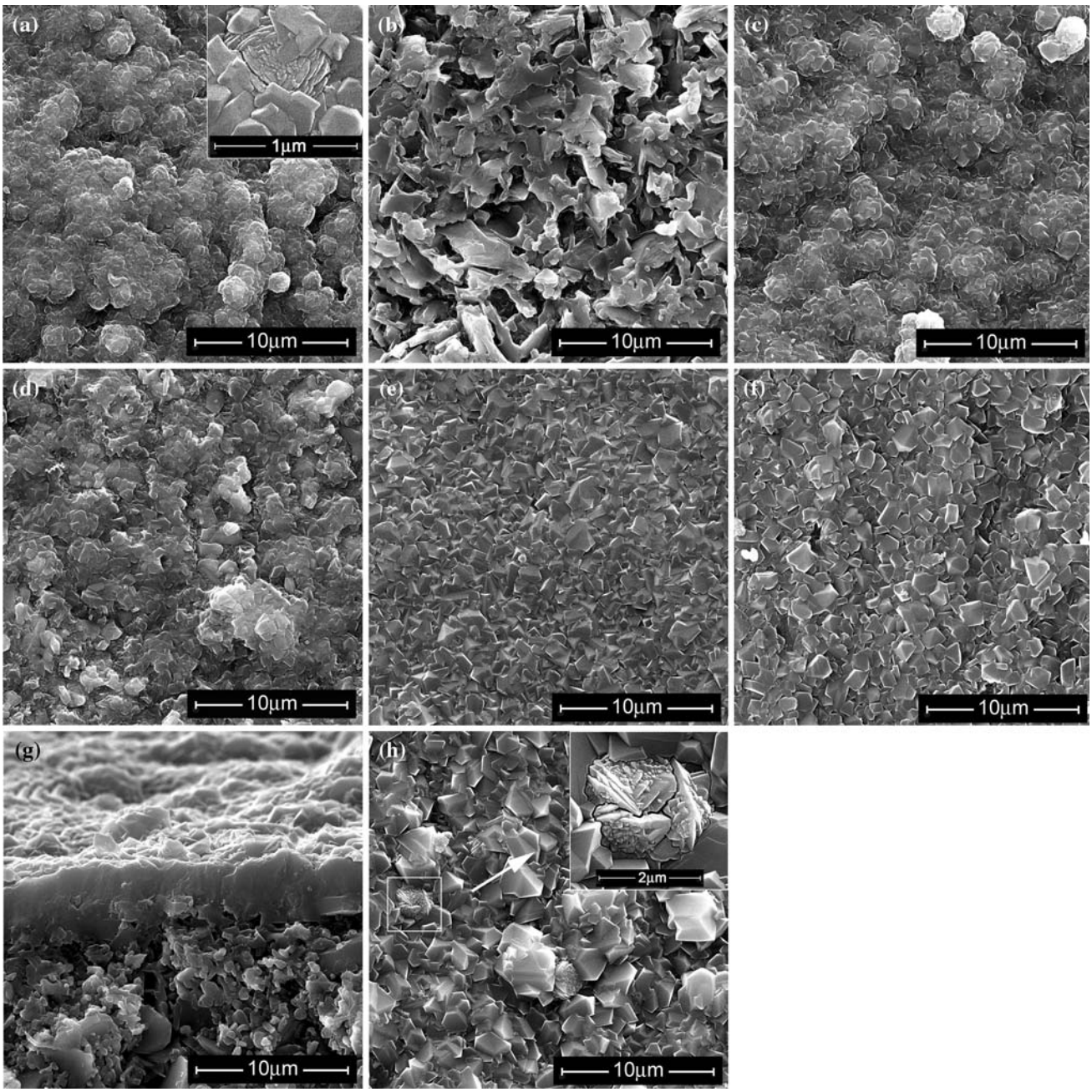

Fig. 6 SEM images of the zeolite layers synthesized with 1 (**a**, **b**), 2 (**c**, **d**), 4 (**e–g**), and 8 h (**h**) of the first stage crystallization (**b**, **d**, and **f** were alkali-treated samples)

could be recognized (inserted image). Figure 6b reveals that these crystals were not firmly attached to the support and could easily fall off after the removal of amorphous materials. A similar layer appearance was observed in Fig. 6c except that the crystals had grown up to 0.5–1 μm and few voids were present. Considerable amorphous materials remained in the zeolite layer, leaving holes and gaps after dissolving in the alkaline solution (Fig. 6d). Further crystallization to 4 h was characterized by a great change in the layer morphology. Uniform crystals with well-developed faces were tightly contacted with each other and they composed a quite smooth surface (Fig. 6e). Visible defects were hardly present in the alkali-treated zeolite layer (Fig. 6f), suggesting that the amount of amorphous materials had significantly decreased by then. At the final stage of crystallization as shown in Fig. 6h, a few walnut-like particles that bore an obviously different morphology with neighbors arose in the zeolite layer. These particles were close to 2 μm in size, and several cracks could be clearly recognized in and around them

from the magnified image. Sato et al. [32] observed the similar walnut-like particles when preparing FAU-type zeolite membranes and took them as P-type zeolite, which could be confirmed by the XRD pattern of 8 h in Fig. 4. These cracks were probably brought by the structure transformation at elevated temperature. There was no significant change in the layer thickness during crystallization, which kept around 5 μm (Fig. 6g). The Si/Na ratio of the zeolite layer increased in the first 2 h, and maintained around 1.3 afterwards (Fig. 5).

After the secondary growth in S2, the pervaporation performances of zeolite membranes synthesized with different first stage crystallization time are shown in Table 1. With the increasing crystallization time, the separation factor first increased, went beyond 350 in the second 2 h, and then gradually decreased. The corresponding flux behaved oppositely, which was high before 1 h and maintained around 1.4–1.5 kg m^{-2} h^{-1} until 8 h when it rose again. Such a trend is consistent with that of $I_{F/S}$ at initial stages and easily understood: in the first hour, crystallization was only partly completed and some relatively large voids remained which could not be eliminated after the secondary growth; on the other hand, P-type zeolite had formed in the zeolite layer by 8 h, which caused the decline of membrane compactness. Although $I_{F/S}$ kept high during 4–8 h, the falling separation performance implied that phase transformation probably had commenced after 4 h, which was slender then whereas got serious after the secondary growth. In conclusion, high-performance membranes could be obtained when the first stage crystallization time was restricted within the second 2 h.

Secondary growth stage

The synthesis solution used for the secondary growth of zeolite layers, i.e., S2, is diluter than S1 and close in composition with the one used by Kumakiri et al. [17]. Their studies revealed that without any substrate or seeds, crystals larger than 0.1 μm did not form in the solution until 7 h of hydrothermal treatment at 80 °C. In their point of view, the secondary growth of seed layers should be restricted to the induction period so as to avoid the exhaustion of reagents on nucleation, and thus they prepared zeolite membranes within 5 h. In this study, we made a detailed investigation on how the secondary growth time influenced the purity and compactness of the zeolite membranes. The first stage crystallization was performed for 4 h.

Figure 7 shows the XRD patterns of the zeolite membranes synthesized with different secondary growth time. In the first 7 h, it seems that the zeolite layers consisted of pure FAU phase as no other peaks could be detected. However, the (101) peak of P-type zeolite arose in the XRD pattern of 9 h, suggesting the occurrence of phase transformation. Figure 8 shows that the $I_{F/S}$ value initially

Table 1 Pervaporation performances of the zeolite membranes synthesized with different first stage crystallization time

Membrane no.	The first stage crystallization time (h)	Pervaporation performances	
		J (kg m^{-2} h^{-1})	$\alpha_{water/ethanol}$
1	0.5	5.15	20
2	1	1.45	150
3	2	1.44	350
4	4	1.48	380
5	6	1.50	180
6	8	1.78	110
7	12	1.82	90

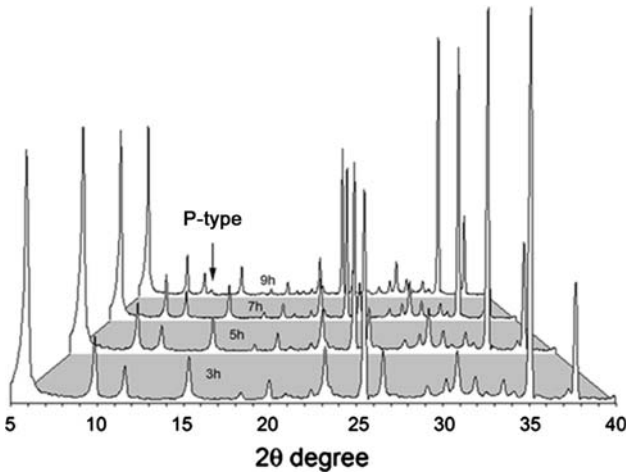

Fig. 7 XRD patterns of the zeolite membranes synthesized with 3, 5, 7, and 9 h of the secondary growth

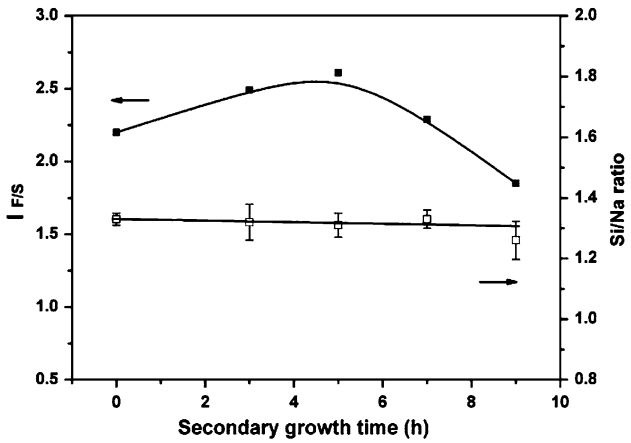

Fig. 8 $I_{F/S}$ and Si/Na ratio as a function of the secondary growth time

increased, reached the maximum at 5 h and then decreased. The Si/Na ratio however kept almost constant around 1.3 during the whole process and corresponded to the Si/Al ratio of NaX type zeolite.

The corresponding SEM images of zeolite membranes are shown in Fig. 9. In the first 5 h, zeolite crystals augmented in size, and moreover they were well intergrown without any visible voids. Figure 9b and d shows that the thickness of zeolite layers increased to around 7 μm. After 7 h, the augment in size continued, whereas some particles with amorphous appearance were present (Fig. 9e). We speculated that these particles were primary P-type zeolite that was probably too small in quantity to be identified by XRD. When prolonging the secondary growth time to 9 h, a lot of walnut-like P-type zeolite crystals strewed the zeolite layer (Fig. 9f), coincident with the XRD result.

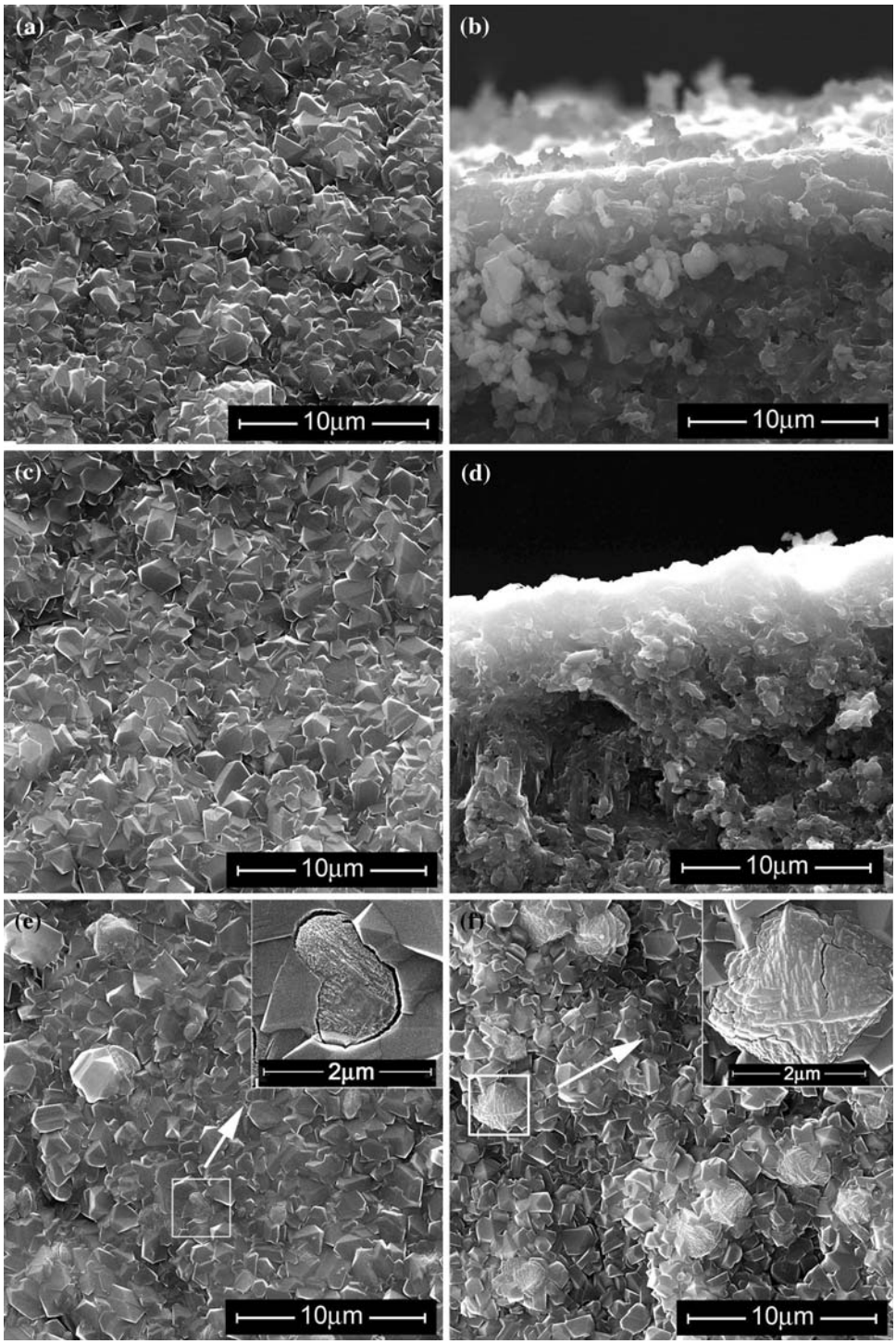

Fig. 9 SEM images of the zeolite membranes synthesized with 3 (**a**, **b**), 5 (**c**, **d**), 7 (**e**), and 9 h (**f**) h of the secondary growth

Table 2 Pervaporation performances of the zeolite membranes synthesized with different secondary growth time

Membrane no.	Secondary growth time (h)	Pervaporation performances	
		J (kg m^{-2} h^{-1})	$\alpha_{water/ethanol}$
8	3	2.65	8
4	5	1.48	380
9	7	1.70	160
10	9	22.6	1.4

Table 2 shows the pervaporation performances of zeolite membranes synthesized with different secondary growth time. The separation factor ascended rapidly to the highest value in the initial 5 h and descended rapidly to almost unit afterwards. Such a result was consistent with the trend of $I_{F/S}$. Thus, it could be deduced that the densification of FAU-type zeolite layer had been completed by 5 h, and further synthesis resulted in a great destruction probably owning to the phase transformation.

Discussion

Effect of aging on suppressing LTA phase

LTA phase is a common by-product in the synthesis of FAU-type zeolite and sometimes they make a competition in the product. Special studies have been carried out on the phase selection of FAU-type and LTA-type zeolites recently [27, 33, 34]. Although it is well accepted that highly alkaline solution makes against the formation of FAU phase, they proposed that sodium cation was also a growth-limiting nutrient. When the pH of synthesis solution was kept constant, the FAU/LTA weight ratio in the product decreased with an increasing content of sodium cation [27]. In order to make a clear solution, the Na_2O/Al_2O_3 ratio of S1 is four times larger in magnitude than those of previous gel solutions. Such a high concentration of alkali and sodium cation probably accounted for the formation of LTA phase during the direct crystallization of FAU-type zeolite membranes. In addition, the dissolution of α-Al_2O_3 support should not be neglected, which reduced the Si/Al ratio of S1 and thus probably aggravated the situation.

Although the element composition of S1 was unchanged during aging, it was effective on suppressing LTA phase mainly by means of the rearrangement of aluminosilicate species. Compared with the dissolution of colloidal silica, the formation of aluminosilicate species was rather fast which was consequently rich in Al and tended to form low-silica zeolite during crystallization [26], i.e., LTA-type. Sufficient aging prior to crystallization produced more siliceous species in liquid phase, which were subsequently incorporated into the aluminosilicate species and concerned with their rearrangement, converting to the precursors of FAU phase. It is therefore easy to explain why relatively high aging temperature and long aging time, i.e., 24 h at 50 °C, led to the formation of a pure phase FAU-type zeolite membrane in view of accelerating the dissolution of colloidal silica. About 60 °C was abandoned in respect that crystallization event had occurred by 8 h owing to the high aging temperature, when the dissolution of colloidal silica was still insufficient. As a consequence, a small amount of LTA-type zeolite formed in the zeolite layer.

Different zeolite phase has different secondary building units (SBUs): LTA phase is mainly composed of 4-membered rings (4R, 2Si2Al), while FAU is 6R (including more Si than Al). It was proposed that 6R and larger membered rings could not be detected and the silicate species was limited in the liquid phase without using templates. During the aging process, siliceous species that were gradually released participated in the evolution of the SBUs from 4R to 6R with higher Si/Al ratio and thus finally resulted in the formation of FAU phase instead of LTA phase [26, 27].

Formation mechanism of FAU-type zeolite membranes

At the end of in situ aging, primary zeolite particles (nuclei) commenced forming in the matrix of the gel layer, which oppositely dissolved and provided nutrients for the growth of zeolite. Therefore, the present in situ aging included not only the induction period but also the initial nucleation of FAU-type zeolite, and consequently promoted the following crystallization at 90 °C.

The first stage crystallization could fall into three stages: formation of crystals by aggregation, Ostwald ripening, and phase transformation. At the initial 2 h, crystallization event was fierce with the promotion of aging. A large number of FAU crystallites were generated and huddled together into aggregates of ca. 1 μm, which could be confirmed by the residual ones in Fig. 6a. These primary crystallites were developed from the aluminosilicate species formed during in situ aging and thus relatively rich in Al. Meanwhile, siliceous species were supposed to be incorporated into the zeolitic framework via liquid phase, resulting in an increasing Si/Al ratio. As these crystallites grew up, they were in close contact with each other and gradually merged into one or several larger crystals. Whereas the merging process took place not only within individual aggregates but also between the ones in close proximity, the pinholes, and gaps gradually shrank and vanished. It was supposed that the nutrients for nucleation and crystallization were mainly provided by the dissolving

Table 3 Pervaporation performances of FAU-type zeolite membranes synthesized by different groups in a water/ethanol (10/90, w/w) mixture

Reporters	Zeolite type (Si/Al ratio)	T (°C)	Pervaporation performances		Membrane performances	
			J (kg m^{-2} h^{-1})	$\alpha_{water/ethanol}$	Water permeance (10^{-6} mol m^{-2} s^{-1} Pa^{-1})	Water/ethanol selectivity
Present work	X (1.3)	65	1.48	380	2.04	470
Kita et al. [12]	X (1.3)	75	1.91	170	1.65	210
	Y (2.1)	75	1.59	130	1.35	140
Kumakiri et al. [17]	Y	30	~0.1	~100	~0.77	~130
Sato et al. [32]	1.4–1.6	75	4–10	110–300	3.6–8.4	64–360

gel in respect that the layer thickness kept almost constant during this evolution.

In the next 2 h, crystallization obviously slowed down mainly by addition of growth units via liquid phase instead of aggregation. Valtchev and Bozhilov [35] considered such a course following aggregation to be Ostwald ripening when studying the formation of FAU-type zeolite. At this stage, the layer surface became smooth and continuous consisting of fairly uniform crystals, and meanwhile the residual amorphous materials were quickly exhausted, which as well as the smaller and less stable zeolite particles dissolved and provided the nutrients for the growth of other crystals.

FAU-type zeolite is metastable and thus tends to crystallize first and then to be replaced by a more stable phase, usually P-type zeolite. As a consequence, after 4 h of crystallization or more, transformation of FAU phase to P-type zeolite took place and caused the decrease in $I_{F/S}$. Although the FAU-type zeolite crystals remained went on growing, the compactness of zeolite layer was destroyed by the increasing amount of P-type zeolite.

The secondary growth of zeolite layers in S2 experienced the growth of crystals and phase transformation. In the first 5 h, the augment in size made the crystals overcrowded and well intergrown with each other. The defects that remained after the first stage synthesis were thus patched up, and the pervaporation performance was enhanced. Whereas no nucleation event took place, the increment of membrane thickness was limited by means of adding growth units. Further prolonging of the secondary growth time again led to the formation of P-type zeolite, and in consequence a rapid decline of separation factor.

Evaluation of the as-synthesized FAU-type zeolite membranes

Table 3 compares the pervaporation process performance and membrane performance [36] of the as-synthesized FAU-type zeolite membrane (Membrane 4) with those of other reports. Membrane 4 possesses the highest water/ethanol selectivity of all, indicating that a high-quality FAU-type zeolite membrane has been prepared by the present in situ synthesis method. Moreover, the water permeance of Membrane 4 is a little higher than the relevant data given by Kita et al. [12], whereas lower than that given by Sato et al. [32]. The reason probably remains with the difference in support type: Sato et al. used asymmetric porous α-Al_2O_3 support, which as well known has the advantage of reducing permeation resistance.

Conclusions

By in situ nucleation and secondary growth, high-quality FAU-type (NaX) zeolite membranes were prepared on porous α-Al_2O_3 tubes from clear solutions. For the in situ nucleation stage, direct crystallization resulted in the formation of LTA phase and poor separation performance, whereas in situ aging could effectively suppress the formation of LTA phase and facilitate the following crystallization. The synthesis time of the first stage crystallization and secondary growth should be restricted in a certain period, or phase transformation to P-type zeolite would occur and depress the separation performance. FAU-type zeolite membranes were composed of well-shaped intergrown crystals, with the thickness of ca. 7 μm. At 65 °C, they exhibited the highest $\alpha_{water/ethanol}$ of 380 and flux of 1.48 kg m^{-2} h^{-1} in a water/ethanol (10/90, w/w) mixture. This convenient in situ synthesis method provides a promising way for the mass production of FAU-type zeolite membranes.

Acknowledgements This work was supported by National Science Fund for Distinguished Young Scholars (20725313), Youth Science Fund of DICP (No. S200609), and the Ministry of Science and Technology of China (Grant No. 2003CB615802).

References

1. Tavolaro E, Drioli E (1999) Adv Mater 11:975
2. Caro J, Noack M, Kölsch P, Schäfer R (2000) Micropor Mesopor Mater 38:3
3. Lin YS, Kumakiri I, Nair BN, Alsyouri H (2002) Sep Purif Method 31:229
4. Bowen TC, Nobel RD, Falconer JL (2004) J Membr Sci 245:1

5. Breck DW (1974) Zeolite molecular sieves: structure, chemistry and use. Wiley, New York, p 73, 168
6. Kusakabe K, Kuroda T, Murata A, Morooka S (1997) Ind Eng Chem Res 36:649
7. Kusakabe K, Kuroda T, Morooka S (1998) J Member Sci 148:13
8. Kusakabe K, Kuroda T, Uchino K, Hasegawa Y, Morooka S (1999) AIChE J 45:1220
9. Guan G, Kusakabe K, Morooka S (2001) J Chem Eng Jpn 34:990
10. Jeong B, Hasegawa Y, Sotowa K, Kusakabe K, Morooka S (2003) J Membr Sci 213:115
11. Kita H, Inoue T, Asamura H, Tanaka K, Okamoto K (1997) Chem Commun 45
12. Kita H, Fuchida K, Horita T, Asamura H, Okamoto K (2001) Sep Purif Tech 25:261
13. Li S, Tuan VA, Falconer JL, Noble RD (2002) Micropor Mesopor Mater 53:59
14. Seike T, Matsuda M, Miyake M (2002) J Mater Chem 12:366
15. Coutinho D, Balkus KJ Jr (2002) Micropor Mesopor Mater 52:79
16. Clet G, Gora L, Nishiyama N, Jansen JC, van Bekkum H, Maschmeyer T (2001) Chem Commun 41
17. Kumakiri I, Yamaguchi T, Nakao S (1999) Ind Eng Chem Res 38:4682
18. Weh K, Noack M, Sieber I, Caro J (2002) Micropor Mesopor Mater 54:27
19. Cheng ZL, Gao EQ, Wan HL (2004) Chem Commun 1718
20. Nikolakis V, Xomeritakis G, Abibi A, Dickson M, Tsapatsis M, Vlachos DG (2001) J Membr Sci 184:209
21. Algieri C, Golemme G, Kallus S, Ramsay JDF (2001) Micropor Mesopor Mater 47:127
22. Zah J, Krieg HM, Breytenbach JC (2006) Micropor Mesopor Mater 93:141
23. Cundy CS, Cox PA (2005) Micropor Mesopor Mater 82:1
24. Wang B, Ma HZ (1998) Micropor Mesopor Mater 25:131
25. Slangen PM, Jansen JC, van Bekkum H (1997) Micropor Mater 9:259
26. Ogura M, Kawazu Y, Takahashi H, Okubo T (2003) Chem Mater 15:2661
27. Fan W, Shirato S, Gao FF, Ogura M, Okubo T (2006) Micropor Mesopor Mater 89:227
28. Li YS, Chen HL, Liu J, Yang WS (2006) J Membr Sci 277:230
29. Li YS, Liu J, Yang WS (2006) J Membr Sci 281:646
30. Nakazawa T, Sadakata M, Okubo T (1998) Micropor Mesopor Mater 21:325
31. Chen HL, Song CS, Yang WS (2007) Micropor Mesopor Mater 102:249
32. Sato K, Sugimoto K, Sekine Y, Takada M, Matsukata M, Nakane T (2007) Micropor Mesopor Mater 101:312
33. Li QH, Creaser D, Sterte J (2002) Chem Mater 14:1319
34. Yang SY, Li QH, Wang MJ, Navrotsky A (2005) Micropor Mesopor Mater 87:261
35. Valtchev VP, Bozhilov KN (2004) J Phys Chem B 108:15587
36. Wijmans JG (2003) J Membr Sci 220:1